Statistics of total electron content depletions observed over the South American continent for the year 2008

G. K. Seemala[1] and C. E. Valladares[1]

Received 25 March 2011; revised 26 July 2011; accepted 4 August 2011; published 29 October 2011.

[1] This paper presents for the first time regional plots of total electron content (TEC) depletions derived from GPS observations over the South American continent with a coverage of over 45° longitude (i.e., 35°W to 80°W). We introduce a new numerical algorithm that has been developed to automatically detect TEC bite-outs that are produced by the transit of equatorial plasma bubbles. This algorithm was applied to TEC values measured by the Low Latitude Ionospheric Sensor Network (LISN) and by receivers that belong to 3 other networks that exist in South America. The general characteristics of the TEC depletions are provided along with their temporal length, local time distribution and depletion depth. The regional day-to-day and seasonal variability of the TEC depletions are also presented for 2008, a year of low solar activity. The regional day-to-day variability of TEC depletions is highly dynamic, but their seasonal distributions follow the longitudinal characteristics of plasma bubbles presented by other authors. During the equinoxes, TEC depletions are mainly observed on the west coast of South America, and during the December solstice they mostly occur on the east side of the continent. However, in all seasons, we observe days when depletions extend all over the continent. We place these new results in the context of theories of plasma bubble seeding.

Citation: Seemala, G. K., and C. E. Valladares (2011), Statistics of total electron content depletions observed over the South American continent for the year 2008, *Radio Sci.*, *46*, RS5019, doi:10.1029/2011RS004722.

1. Introduction

[2] Measurement of total electron content (TEC) values using dual-frequency GPS receivers has become a reliable and cost effective method to probe the thermosphere-ionosphere system. A single GPS receiver measures the line-of-sight integrated electron content from 6 to 12 GPS satellites simultaneously and continuously. Multiple GPS receivers, forming regional or global networks, map the integrated number densities over large areas, complementing near-Earth satellites or non-scanning radars, and provide a more complete view of the ionospheric background conditions. Recently, *Basu et al.* [2005] and *Foster et al.* [2005] have used global maps of TEC to investigate the ionospheric dynamics at mid and high latitudes during magnetically disturbed periods. *Valladares et al.* [2001, 2004] employed a chain of 12 GPS receivers in South America to derive TEC latitudinal profiles extending ±30° on both sides of the magnetic equator. They associated the location of the crest of the equatorial anomaly and the altitude of the *F* region, measured by the Jicamarca Digisonde, with the development or lack of equatorial plasma bubbles (EPB). Regional maps of TEC perturbations (TECP) have been used to diagnose and study the morphology of atmospheric gravity waves (AWG) that are produced at high latitudes during magnetic storms [*Ho et al.*, 1998; *Saito et al.*, 1998; *Shiokawa et al.*, 2002; *Valladares et al.*, 2009]. TEC values provided by dense networks of GPS receivers have also been used to reconstruct three-dimensional maps of ionospheric densities [*Ma et al.*, 2005; *Lee et al.*, 2007, 2008; *Mitchell and Spencer*, 2003]. Other studies have presented perturbations of the daily TEC values containing periods of about 1 h or less. TECP are mainly associated with atmospheric gravity waves (AGW) as they move the *F* region plasma up and down the magnetic field lines. Plasma bubbles can also produce perturbations in the TEC values as they move according to the background E × B field. *Conker et al.* [2004], *Rama Rao et al.* [2006], and *Portillo et al.* [2008] have designed methods to detect TEC perturbations associated with the drifting bubbles.

[3] In this paper, we present the results of a statistical study of TEC depletions observed with 127 receivers that operated in South America in 2008. We have observed TEC depletions having periods between 10 and 120 min. Typically, a series of perturbations can be seen in a single day lasting for several hours. At low latitudes, nighttime TECP are also produced by EPBs. However, they are readily identified by their typical sudden decreases that can reach values in excess of 10 TEC units. As indicated above, TEC perturbations can also be generated by the passage of AGW originated in the troposphere by weather systems. However, this type of TECP has a marked sinusoidal nature with periods between 10 min and 1 h, duration of a few hours and

[1]Institute for Scientific Research, Boston College, Chestnut Hill, Massachusetts, USA.

0048-6604/11/2011RS004722

amplitudes smaller than 1 TEC unit. These characteristics can be used to identify them.

[4] It is known that near sunset, the dynamics of the equatorial ionosphere are dominated by the pre-reversal enhancement (PRE) [*Woodman and LaHoz*, 1976] of the vertical drift. During sunset, plasma densities and dynamo electric fields in the *E* region decrease, and the anomaly begins to fade, and at this local time a dynamo electric field develops in the *F* region. Polarization charges, set up by the conductivity gradients at the terminator, enhance the eastward electric field for about an hour after sunset. This eastward post-sunset electric field enhances the Rayleigh-Taylor (R-T) instability, while a westward field quenches it. These structures can grow to become large-scale ionospheric depletions, often called equatorial plasma bubbles, which are elongated along the magnetic flux tubes. The variability in the PRE may dictate the onset or inhibition of these instabilities [*Basu et al.*, 1996; *Hysell and Burcham*, 1998; *Fejer et al.*, 1999].

[5] The statistical study of TEC depletions presented here is motivated by the need to understand the onset of equatorial plasma bubbles. EPB has long been recognized as one of the most prominent concerns of space weather. EPB is responsible for the degradation of radio propagation that leads to navigation errors and outages, communication system failures and radar clutter. Previous statistical studies of the occurrence of plasma bubbles, using in situ density measured by the Defense Meteorological Satellite Program (DMSP) satellites, implied strong variability of their occurrence across South America during the equinoxes and December solstice months [*Burke et al.*, 2004; *Huang et al.*, 2001]. It is expected that a similar occurrence, but containing higher spatial and temporal resolution, will result from the statistics of TEC depletions as we are examining the same phenomena. During 2008, the Low-latitude Ionospheric Sensor network (LISN) operated 29 receivers installed in the countries of Argentina, Brazil, Colombia, and Peru. These receivers had Internet connectivity and were able to upload near real-time data to a central server located at the Instituto Geofisico del Peru in Lima. This paper is organized in the following fashion. Section 2 shows typical TEC depletions observed by GPS receivers placed at different magnetic latitudes as they move eastward across South America. Here, we describe the procedures that were developed to identify EPB. Section 3 introduces the reader to maps of TEC depletions seen on individual days. The statistics of TEC depletions are shown in section 4. We end the paper with the discussion and summary sections.

2. TEC Depletions

[6] TEC depletions consist of abrupt decreases in the TEC value that last from 10 to 60 min. They are commonly followed by a recovery to the TEC value preceding the depletion. The TEC depletions that we are considering are produced by plasma bubbles drifting across the line-of-sight between the GPS receiver and the satellite. *Weber et al.* [1996] showed a strong correlation between TEC depletions and airglow 630.0 nm depletions, implying that TEC depletions are manifestation of equatorial plasma depletions. The general morphology of TEC depletions and their association with strong levels of VHF scintillations were described by *DasGupta et al.* [1983] for the pre-midnight period. *Yeh et al.* [1979] have reported similar correlations in the occurrence of bubbles and scintillations.

[7] Figure 1 shows the locations of all 127 dual-frequency GPS receivers stations used in this study. They were deployed by LISN, Ohio State University - Central and Southern Andes GPS Project (OSU-CAP), Geocentric Reference System for the Americas (SIRGAS) [*Brunini et al.*, 2011] and International GNSS service (IGS) [*Dow et al.*, 2009] networks. These GPS receivers cover most of the South American continent with longitude coverage between 35° and 80° West and geographic latitudes in the range of 45°S to 13°N, (magnetic latitudes in the range of 35°S to 20°N). The calculation of the equivalent vertical TEC was done independently for each of the GPS receivers using an analysis code that was developed at Boston College. This program uses the phase and code values for both L1 and L2 GPS frequencies to eliminate the effect of clock errors and tropospheric water vapor to calculate relative values of slant TEC [*Sardón and Zarraoa*, 1997]. Then, the absolute values of TEC are obtained by including the differential satellite biases published by the University of Bern and the receiver bias that is calculated by minimizing the TEC variability between 0200 and 0600 LT [*Valladares et al.*, 2009; P. Doherty, private communication, 2000].

[8] We have developed a software code that is able to automatically identify the TEC depletions by examining the TEC trace for each GPS satellite pass individually and for each of the 127 stations in South America. The algorithm identifies depletions by separating the spectrum of depletion structures from the one corresponding to the variability of the background or unperturbed TEC. Most of the time, the durations of observed TEC depletions lie within the range of 10 to 60 min. We first used a single digital Band Pass Filter (BPF) with cut-off values from 3 min to 120 min and realized that this was not very effective due to false detections produced by rapid (less than 2 h) variations of the background TEC and steep horizontal gradients. Hence the depletions are detected by using two digital BPFs, one to get structures of depletions whose observed durations are between 3 min and 40 min and the second BPF to detect wider depletions with duration between of 25 min and 120 min. These are equivalent to cutoff frequencies of both filters between 1.4×10^{-4} and 6.7×10^{-4} Hz for the first BPF and also 4.2×10^{-4} and 56×10^{-4} Hz for the second BPF. This separation of a spectrum range of 3 to 120 min into two overlapping spectrum of structures avoids the false detection of depletions from the structures that are caused by steep gradients in TEC, and is also useful in emphasizing individually narrow and wider depletions, raising their thresholds levels in each case for easier detection. The depletions per se are detected from the filtered amplitudes whose threshold values fall below −1 TEC and −0.6 TEC units respectively for narrow and wide depletions. The bubble detection is confirmed if the observing elevation angle is above 30° and TEC recovers to a value closely similar to the starting TEC. Initial and end times of the TEC depletion are determined by selecting the times when the slope of the filtered TEC value becomes different than zero and before the TEC moves beyond the negative threshold value and after it resumes a positive value respectively. These identified depletions are validated by their onset times (post sunset time), geomagnetic location of

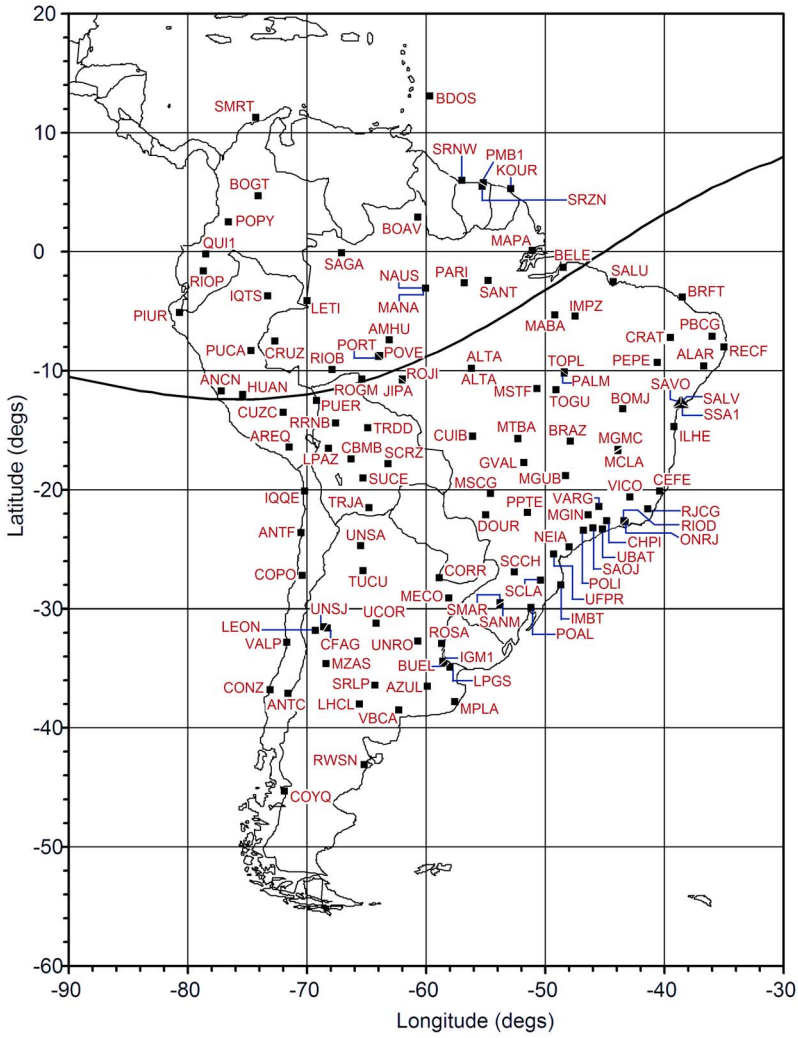

Figure 1. Locations of GPS receiver stations installed by the LISN, OSU, SIRGAS and IGS networks in the South American continent that are used in this study. Black solid squares represent station locations along with 4 letter station codes.

occurrence and false detections arising due to TEC gradients at low elevation angles and data breaks. The following subsections present several cases of TEC depletions observed in 2008 to illustrate the variety of conditions in which depletions develop and the complex relationship that exists between the depth, the width of a depletion, wall steepness, background TEC values and the S4 index.

2.1. Antofagasta, Chile, 9 October 2008

[9] Figure 2 shows the TEC values recorded at Antofagasta, Chile from GPS PRN 26 on 9 October 2008. Figure 2 displays typical TEC depletions detected near the southern crest of the anomaly that are accompanied with significant levels of scintillations. This case was selected due to the easiness to determine the boundaries of the depletions. Two adjacent TEC depletions are observed on this pass. Figure 2a shows the spectra of the TEC values that are used to confirm the nature of the TEC variability. Two spectral bands are indicated and depicted by the pink and blue lines. These bands correspond to periods between 25 and 120 min (pink), 3 and 40 min (blue) for wide and narrow depletion detection, respectively. Figure 2b shows the TEC value (green trace), elevation angle (orange trace) and the corresponding S4 scintillation indices (red trace). S4 is obtained by measuring the standard deviation of normalized GPS signal power (S/N amplitude) at 50 Hz sampling. There is an excellent correspondence between the TEC depletion and the S4 values above the noise level (S4 ≈ 0.1). Figure 2c displays the TEC values after they have been band-pass filtered using the filter bands indicated in Figure 2a. These two traces, blue (values of first filter or narrow depletion BPF) and pink (values of second filter or wide depletion BPF) are used to detect the TEC depletions. These two depletions indicated in Figure 2b are detected from filtered values of the first BPF as the values decreased beyond threshold value (−1.0) and resumed positive. The start times (indicated by the blue vertical line in Figure 2b) of the TEC depletions were determined when the slope of the filtered values of the first BPF (Figure 2c, blue trace) becomes negative while the filtered TEC values are still positive. The end times (indicated by orange vertical line in Figure 2b) were identified when the slope of the filtered values becomes zero or very small after the filtered TEC

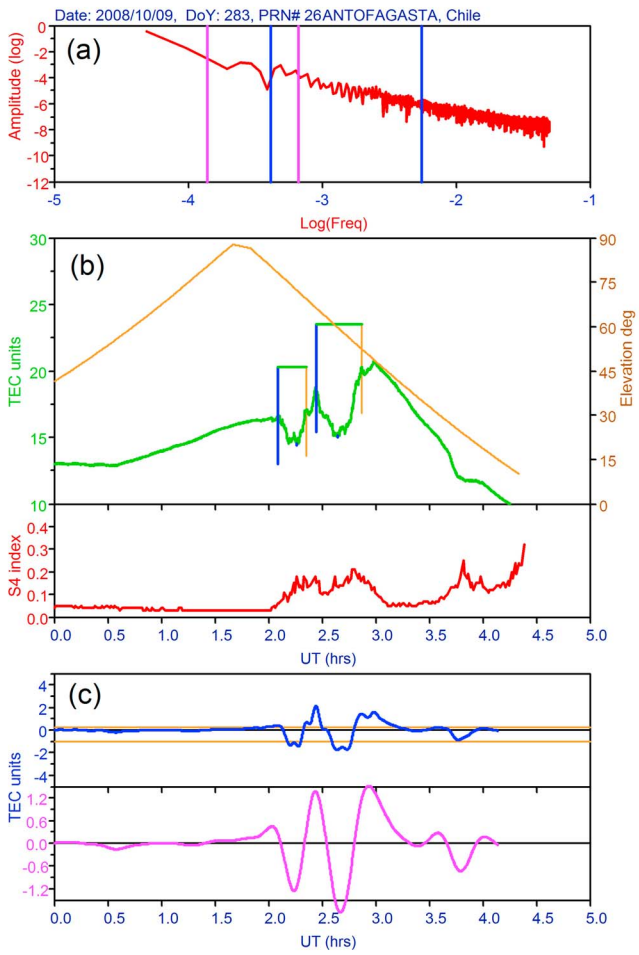

Figure 2. Automatic detection of TEC depletions from the calculated TEC values of GPS satellite (PRN 26) on 9 October 2008. (a) The spectra of TEC values with band pass filter cut-offs indicated by pink (filter 1) and blue (filter 2) vertical lines. (b) Observed TEC values (green) along with elevation angle (orange) marked with identified depletions between blue and orange vertical lines. (c) The outputs of the BPFs indicated by blue trace from filter 1 and pink trace from filter 2.

values resume positive. Both TEC depletions were observed when the viewing angle was above 45° elevation. Followed by these two depletions, the filtered values (pink trace in Figure 2c) cross the threshold between 0330 and 0400 UT, but it was not indicated as valid depletion as it is eliminated by the elevation mask angle of 30°. It is important to mention that multipath can also produce artificial signal fluctuations that may originate elevated S4 values. However, these multipath-enhanced S4 indices occur when the satellite elevation angle is below 30° as it is observed near 0400 UT.

2.2. Ancon, Peru, 13 February 2008

[10] Figures 3a and 3b present TEC depletions recorded on the same day, containing similar levels of unperturbed TEC values, at stations located near the magnetic equator but separated by 21° in longitude. The level of Scintillation S4 index within the depletions varies drastically. Figure 3a shows the TEC recorded at Ancon, Peru, for PRN 16 on 13 February 2008. Ancon (11.77°S, 77.15°W) is located near the magnetic equator on the west coast of South America. Two depletions are identified in this pass; no scintillation above the noise level is observed for the first depletion, which may be attributed to the smaller TEC gradients at the edge of the depletion. A moderate scintillation patch of about S4 = 0.2 is observed in correspondence with the second depletion when the satellite elevation angle is more than 60° and has much steeper TEC gradient than the first depletion. It is mentioned that the highest S4 values were observed on the eastern side of the depletion. As the plasma depletion is drifting eastward and faster than the apparent east-west motion of the satellite sub-ionospheric intersection (<10 m/s), the eastern side of the depletions is commonly observed first.

2.3. Alta Floresta, Brazil, 13 February 2008

[11] The TEC depletion of Figure 3b demonstrates that even during low solar conditions, significant levels of scintillations can be observed near the magnetic equator. Figure 3b shows TEC values from the equatorial station, Alta Floresta (9.8°S, 56.1°W), which is 3° south of magnetic equator and in the middle of South America. At the beginning of the pass there exists a moderate level of scintillations (S4 = 0.3), which is due to multipath as the elevation angle is lower than 30°. A single depletion is detected at elevation angle above 30° and has a corresponding scintillation of about S4 = 0.3 that is well separated from the multipath scintillation patch. Here, the scintillation intensity corresponding to this depletion is higher than the S4 detected at the equatorial station of Ancon on the same day.

2.4. Boa Vista, Brazil, 2 February 2008

[12] The TEC depletion of Figure 3c was recorded near the northern crest and characterized by a depth larger than 10 TEC units. The wider and deeper depletion is associated with larger levels of scintillations. Figure 3c presents TEC values from the anomaly station Boa Vista (2.8°N, 60.6°W) for GPS PRN 12. The depletion detected has a sharp gradient and a depth of about 14 TEC units, which is more than 50% of the total TEC before the depletion started. The width of the depletion is 39 min and is associated with strong levels of scintillation that reach a maximum of S4 = 0.47 (>10 dB) when the elevation angle of the satellite is 45°. The scintillation is present for the entire duration of the depletion and extending for about 15 min beyond the detected end of the depletion.

2.5. Dourados, Brazil, 7 November 2008

[13] The TEC depletions of Figure 3d were accompanied by a stronger level of scintillation than Figure 3c that generated a loss of signal by 25 min. Figure 3d shows an example of a deep depletion and strong scintillations that were observed at the anomaly station of Dourados (22.1°S, 54.9°W). There are two depletions in the TEC data, but only one depletion was detected by the program. The second depletion (UT ~0200) was not detected due to the loss of L2 signal probably related to the deep fading associated with the high scintillation activity at the second depletion. The first depletion is associated with strong scintillations S4 = 0.5 (>10 dB) at elevation angle of 40° and has large electron density at both edges of the depletion. The second depletion started within few minutes after the first is also accompanied

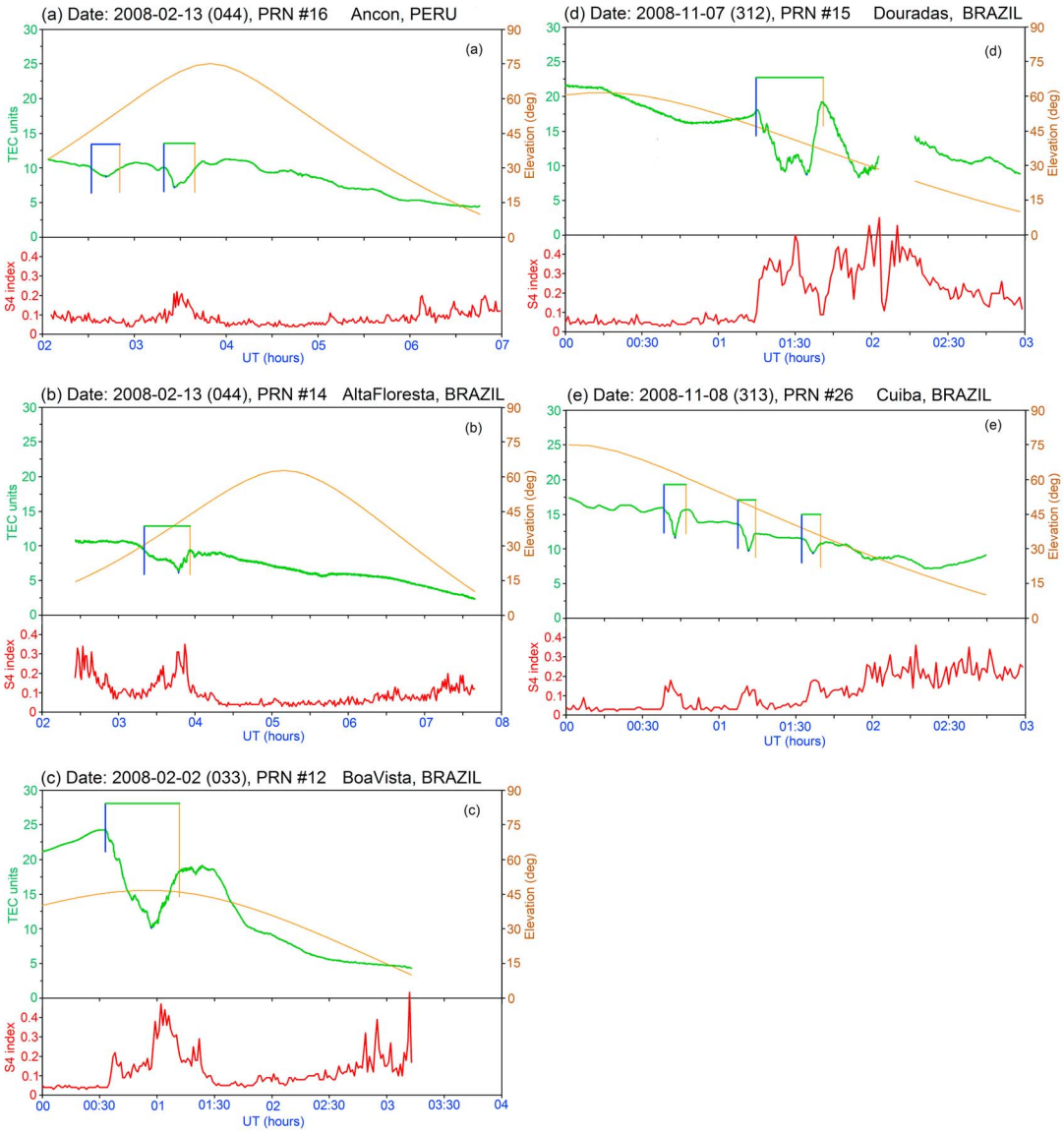

Figure 3. TEC and scintillations observed at (a) Ancon, Peru, on 13 February 2008 from PRN 16, (b) Alta Floresta, Brazil, on 13 February 2008 from PRN 14, (c) Boa Vista, Brazil, on 2 February 2008 from PRN 12, (d) Dourados, Brazil, on 11 November 2008 from PRN 15 and (e) Cuiba, Brazil, on 8 November 2008 from PRN 26.

by strong scintillations S4 > 0.6 at elevation angle of about 30°. Due to the depth and length of the second depletion, the receiver lost lock on the L2 signal and TEC was not calculated during this time. Figure 3d points out the fact that the large scintillation associated with the plasma bubbles can cause loss of lock of GPS receivers even during solar minimum conditions when TEC is commonly below 30 TEC units at anomaly stations.

2.6. Cuiba, Brazil, 8 November 2008

[14] The automatic detection of the narrow (15 min) multiple TEC depletions of Figure 3e are confirmed by the level of scintillations that slightly exceeds the noise level. Figure 3e shows TEC from the anomaly station Cuiba (15.5°S, 56.07°W) for PRN 26 on 8 November 2008. Three depletions are detected from this satellite pass, and these depletions have good correspondence with the occurrence of scintillation patches. The scintillation patch corresponding to the third depletion, which is above the elevation angle of 30° shows S4 index equal to 0.2. The morphology of the S4 enhancement is distinct from the noise level and the S4 that is associated with multipath for elevation angles less than 30°, as seen after 0200 UT.

3. Day to Day Variability of TEC Depletions

[15] One of the most successful hypothesis to explain the longitudinal/seasonal occurrence of equatorial spread-F (ESF) was proposed by *Tsunoda* [1985]. Tsunoda indicated that ESF activity increases when the solar terminator aligns with the geomagnetic field ***B***. For example, equinoxial maxima exist at longitudes where the B lines align with a

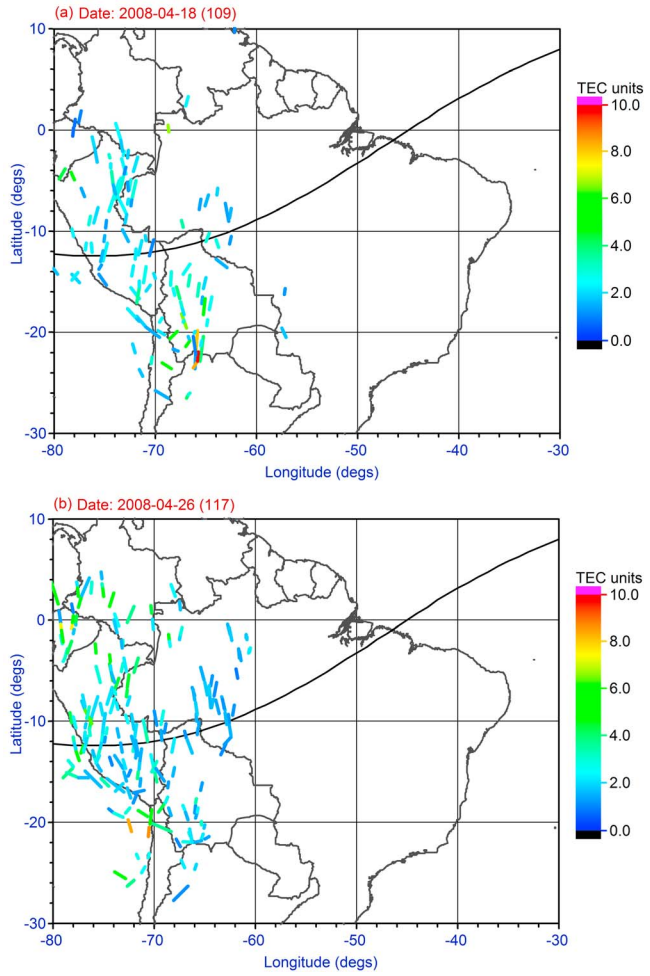

Figure 4. Depletions detected from all GPS receivers over South American continent on (a) 18 April 2008 and (b) 26 April 2008. This shows the most typical pattern during Equinox.

geographic meridian (i.e., west coast of South America). During the December solstice the maximum occurs at longitudes where the B field declination is westward as it happens over the eastern part of Brazil. This effect can be understood in terms of sunset not occurring simultaneously at both conjugate *E* regions. Over the sunlit hemisphere, the *E* region ionization can short circuit the polarization electric field that develops during the evolution phase of the ESF irregularities and is equally effective on inhibiting the electric field associated with the pre-reversal enhancement.

[16] As indicated above, in the South American region, the solar terminator alignment with magnetic field lines varies strongly with longitude. As a result, the highest occurrence of scintillation should be in the western side of South America (Peruvian region) during Mar/April and Oct/Nov, and in the eastern side of South America (eastern Brazil) between December and February.

3.1. Depletion Occurrence on 18 and 26 April 2008

[17] Figures 4a and 4b show the spatial distributions of detected depletions from all the GPS receiver stations in South American region for 18 and 26 April 2008, respectively. The depletions identified in these plots correspond to the time window of 2200 UT to 0700 UT of the following day. This universal time interval covers local time between sunset and few hours after midnight in the South American longitudes. The colored segments are the GPS satellite tracks at the ionospheric pierce point for the altitude of 350 km. Each segment represents the line joining the start and end points of depletion identified region from each of the GPS satellites. The color coding is done according to the depth of the detected depletion in TEC units as in the color scale. All the TEC depletions in Figure 4 were not unique; they might have been detected simultaneously by two or more GPS satellite signals that have their line of sight intercepted through the same plasma depletion but at different latitudes. Therefore, the number of TEC depletions detected might be more than the actual number of plasma bubbles in the region, and each of the identified bubbles may have a different duration and magnitude depending on their intersection with satellite path and elevation with plasma depletion. Due to the relatively slow east-west motion of the GPS satellites, we can say that the plasma depletions are traversing a quasi-stationary receiver-satellite link. The depletion duration identified from GPS TEC is a function of the bubble width and the satellite elevation.

[18] In Figure 4a, the identified depletions on this day of 18 April 2008 have depletion depths falling into ranges of 1 to 4 TEC units, and most of these are along the longitude range of 80° to 60°W. These depletions have the apparent onset times (as observed by the satellite signal) between 2100 to post midnight 0100 LT. The onset times were not represented in these figures.

[19] Figure 4b shows the depletions detected on 26 April 2008 with depths varying from 2 to 7 TEC units. The depletions on this day can be identified from two different ionospheric irregularities depending on their onset times. The depletions in the longitude range of 80° to 70°W were detected between about 1930 to 2200 LT; and those in the longitude range of 70° to 60°W have onset times of 2300 to 0100 LT. The depletions with slightly larger TEC depths are concentrated into the anomaly regions. It can be seen from Figures 4a and 4b, that the depletions identified over the South American region are concentrated in the western South American region with no occurrence in the eastern side for these two days. The depletion behavior presented in Figures 4a and 4b follows the *Tsunoda*'s [1985] hypothesis of solar terminator – magnetic meridian alignment. But, there are also some days during that equinoxes that will not follow this hypothesis.

3.2. Depletion Occurrence on 9 and 19 March 2008

[20] Figure 5a shows the depletions detected on 9 March 2008 over the South American region. Most of the depletions in the eastern longitudes have the TEC depths in the range of 3 to 8 TEC units. The apparent onset times for this day are about 2100 to post midnight 0100 LT. Figure 5b shows the depletions detected on 19 March 2008 over the South American region, which shows consistent spread of identified depletions over all longitudes with concentrated numbers around the anomaly crest regions. The depletion depths are in the range of 1 to 6 TEC units with some depletions peaking up to 8 TEC unit depths near the regions around the anomaly crests. The onset times for this day are

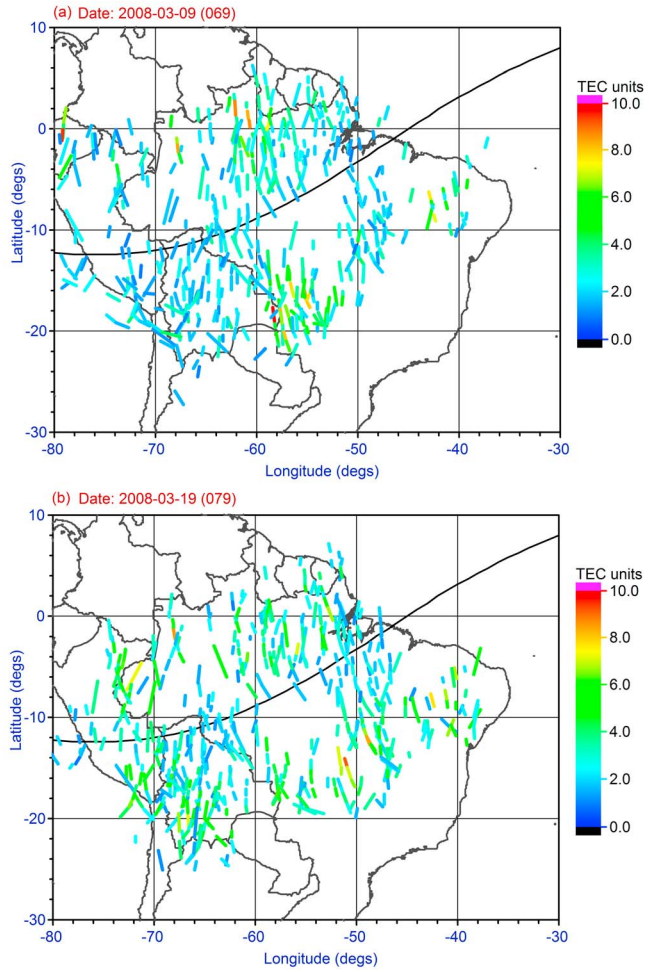

Figure 5. Depletions detected from all GPS receivers over South American continent on (a) 9 March 2008 and (b) 19 March 2008.

in the range of 2000 to post midnight 0100 LT. The TEC depletions for these two days clearly show that the occurrence of depletions at all longitudes in the South American region does not follow the solar terminator – magnetic meridian alignment hypothesis. The effect of solar terminator alignment with magnetic field on occurrence of depletions can be seen statistically over a month but it was not consistently observed on a day-to-day basis.

3.3. Depletion Occurrence on 3 and 10 December 2008

[21] Figures 6a and 6b, corresponding to 3 and 10 December 2008, show most of the TEC depletions concentrated in the eastern longitudes of the South American region with practically no depletions in the western side. They have the onset times in the range of 2030 to 0030 LT. This behavior follows Tsunoda's hypothesis of the solar terminator – magnetic meridian alignment, which is true for most of the days in December solstice. The depletion depths of these two days are in the ranges of 2 to 8 TEC units. On 10 December 2008 (Figure 6b) there are two concentrated groups of depletions identified which are possibly due to two different irregularity regions with different onset times; the longitudes 45°W to 34°W are in the range of 2000 to 2200 LT and the longitudes 58°W to 45°W are from 2230 to 0130 LT.

3.4. Depletion Occurrence on 10 January and 14 December 2008

[22] Figures 7a and 7b show the depletions detected on 10 January and 14 December 2008, respectively, over the South American region. During these two days the depletions are identified at all longitudes across the continent, even at regions where the solar terminator hypothesis does not predict depletions for the December solstice. It can be seen that there exists 3 bands of concentrated number of depletions identified along the longitude ranges of 48°W, 55°W and 65°W. These depletions have onset times between about 1930 and 2330 LT. On 14 December 2008 the onset times of depletions for longitudes 50°W to 35°W are in the range of 2000 to 2300 LT and for longitudes 75°W to 55°W are about 2000 to 2200 LT.

3.5. Depletion Occurrence on 27 June and 13 July 2008

[23] Figures 8a and 8b show the depletions detected on 27 June and 13 July 2008, respectively, over the South

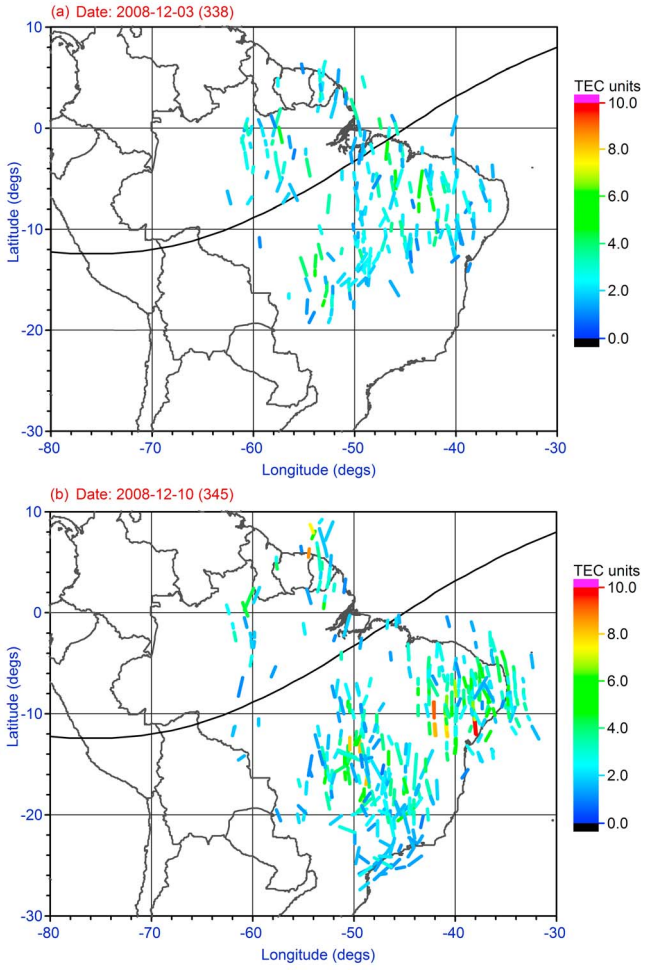

Figure 6. Depletions detected from all GPS receivers over South American continent on (a) 3 December 2008 and (b) 10 December 2008. This represents typical pattern during December solstice.

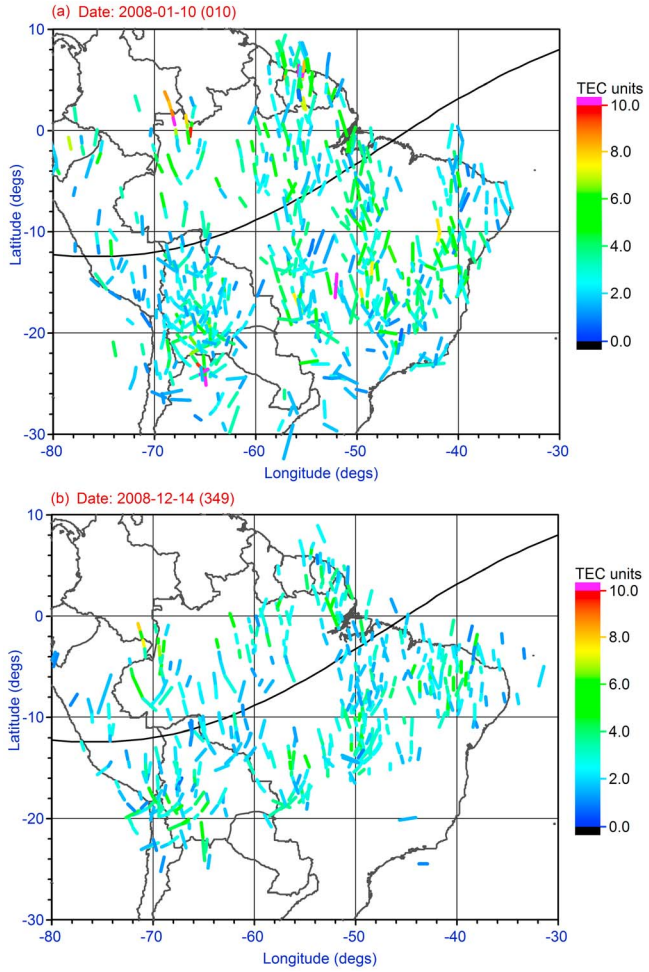

Figure 7. Depletions detected from all GPS receivers over South American continent on (a) 10 January 2008 and (b) 14 December 2008.

American region. The onset times for the plasma depletions of 27 June (Figure 8a) are 2100 to 2300 LT and for 13 July (Figure 8b) are 2330 to 0030 LT. 27 June 2008 is the day when more TEC depletions were identified than any other day during this solstice period. It is well known that during the June solstice very few plasma depletions are observed over the South American region unlike the December solstice which has maximum occurrence of depletions over the eastern part of the continent.

3.6. Depletion Occurrence on 11, 12, and 14 February 2008

[24] Figures 9a, 9b, and 9c present the depletions identified on closely consecutive days of 11, 12, and 14 February 2008 showing different patterns of depletion detections in the South American region. On 11 February 2008 (Figure 9a) the depletions are identified in the eastern longitudes of the South American continent, with onset times of about 2130 to 0030 LT, with depletions depths in the range of 1 to 4 TEC units. On 12 February 2008 the depletions are detected in the western longitudes of the South American region with onset times of about 2100 to post midnight 0130 LT, with depletions depths in the range of 1 to 6 TEC units. On 14 February 2008 (Figure 9c) the depletions were identified at all longitudes over South America, the onset times for longitudes between 60°W and 40°W was 2000 to 2200 LT and for longitudes between 80°W to 60°W was about 2100 to post midnight 0130 LT. The range of depletion depths on this day is from 2 to 10 TEC units. Deeper TEC depletions were observed near both anomaly crest regions.

4. Statistics of Depletions

[25] The TEC data used in this study come from the GPS receivers shown in Figure 1. They cover most of South America with some coarse coverage at the northern and southern parts of the continent due to the sparsity of receivers in those regions. The coverage provided by the GPS satellite constellation over a particular location remains the same throughout the year, as the GPS satellites return to the same place every 23 h and 56 min. Therefore, the statistics of TEC depletions detected with GPS receivers have similar number of samples. The following two sub-sections describe the statistics of the TEC depletions observed on 2008.

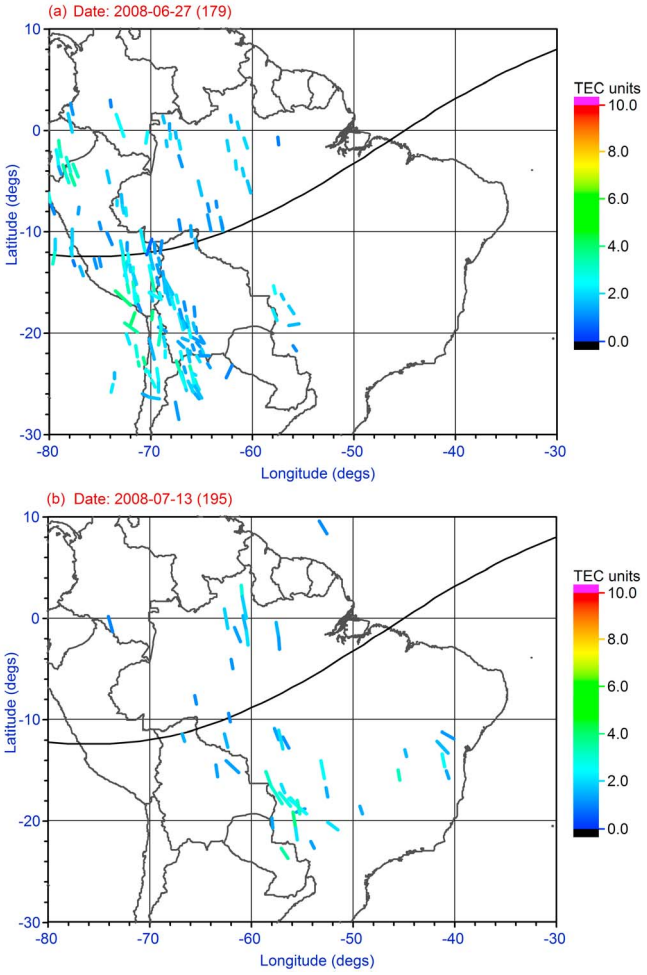

Figure 8. Depletions detected from all GPS receivers over South American continent during June solstice on days of (a) 27 June 2008 and (b) 13 July 2008.

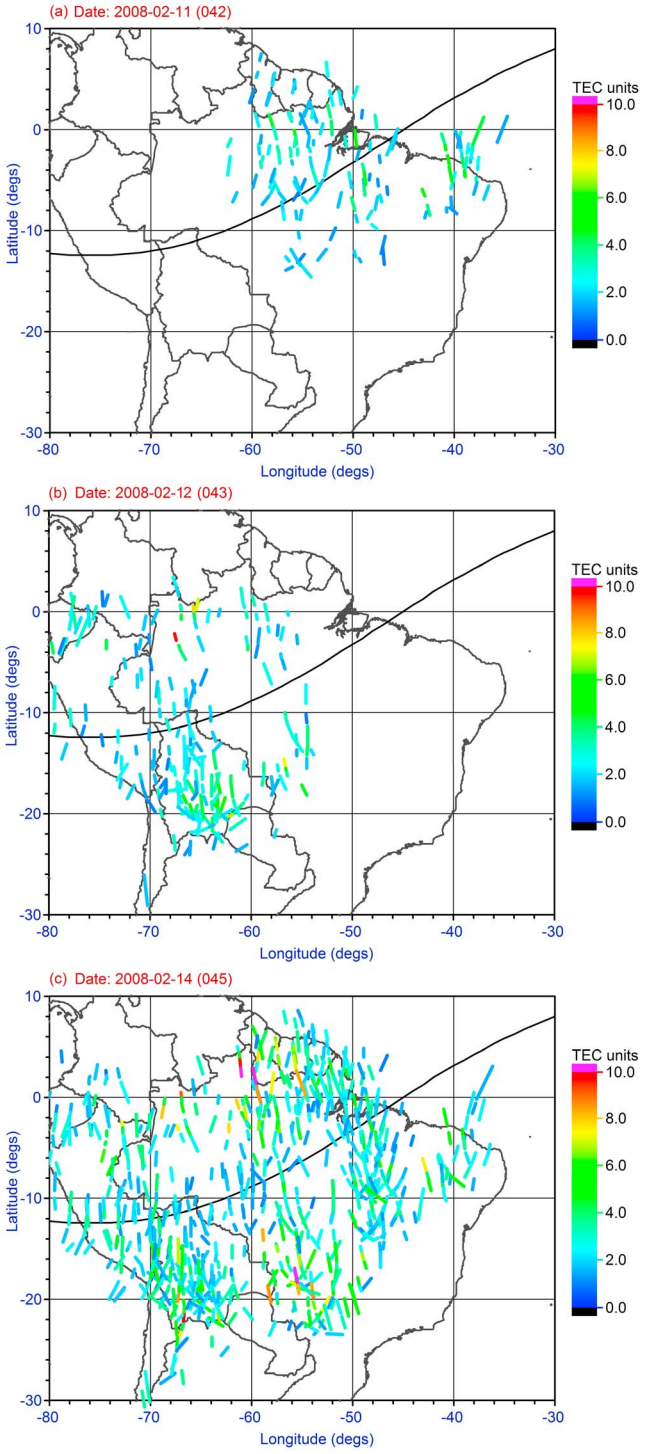

Figure 9. Spatial TEC depletion patterns on the three consecutive days that depict the dynamics of depletion occurrence, which is a contradiction to the hypothesis of solar terminator alignment as suggested by *Tsunoda* [1985].

4.1. Seasonal and Longitudinal Variability of Depletions

[26] The magnetic declination of the Earth's magnetic field varies sharply across South America, consequently, the degree of alignment between the solar terminator and the magnetic field shows a markedly different seasonal morphology at the western and eastern coasts of the continent. Following *Tsunoda*'s [1985] argument, the occurrence of TEC depletions will increase in the Peruvian sector during the equinoxes, but will maximize in eastern Brazil during the December solstice. Figures 10a and 10b show our statistical results on the number of TEC depletions for the months of March 2008 (equinox) and December 2008 (solstice) respectively. These contour plots show the TEC depletions that were observed at grid points with a size of 1° by 1°.

[27] Figure 10a shows the maximum number of depletions concentrated in the longitude range between 70°W and 63°W (greater than 70 TEC depletions). The eastern longitudes display a low depletion occurrence (less than 25 TEC depletions). It is important to note that the peak number of depletions was observed at grid points corresponding to the statistical location of the southern crest of the anomaly region where the densities are larger and the depletions easier to be identified. It is evident that the monthly maximum of TEC depletions concurs with the seasons when the solar terminator aligns with the magnetic field.

[28] Figure 10b shows the maximum number of depletions (about 80 TEC depletions) in the longitude range of 55°W to 35°W at latitudes collocated with the southern anomaly crest region. The number of TEC depletions is much reduced in the western longitudes. In summary, Figures 10a and 10b demonstrate that more TEC depletions develop in the western side of South America during the Equinoctial month of March and in the eastern side during December, all in agreement with satellite observations [*Burke et al.*, 2004] and theoretical predictions [*Tsunoda*, 2010a]. We also observed more TEC depletions in December than March for 2008, a year of low solar activity.

[29] Figure 11 shows the longitudinal distribution of depletions for year 2008 observed over the South American continent. The contour plots are drawn from the total number of depletions occurring at each longitude bin of 1°, including depletions that were observed at all latitudes for every day of 2008. The colors represent the number of TEC depletions in geographic coordinates. Figure 11 clearly shows the two maxima of depletion occurrence at the equinoxes and December solstice which is similar to the one shown by *Burke et al.* [2004] and follows the solar-terminator-B alignment (STBA) hypothesis of *Tsunoda* [1985]. The longitudinal distribution of depletions clearly shows a pattern that maximizes at western longitudes during the equinoxes and at eastern longitudes during December solstice. During the month of October, we can see TEC depletions transitioning from western to eastern longitudes. A similar effect is seen between mid-January and February when TEC depletion development transits from eastern to western longitudes. During June solstice months (May, June, July, August) the number of TEC depletions is almost null except for a few days that showed TEC depletions on the western side of South America.

[30] During the low solar activity year of 2008, Figures 10a and 10b have shown that we observed 20% more TEC depletions during the December solstice than the March equinox. However, we recorded approximately the same number of satellite passes during these two months.

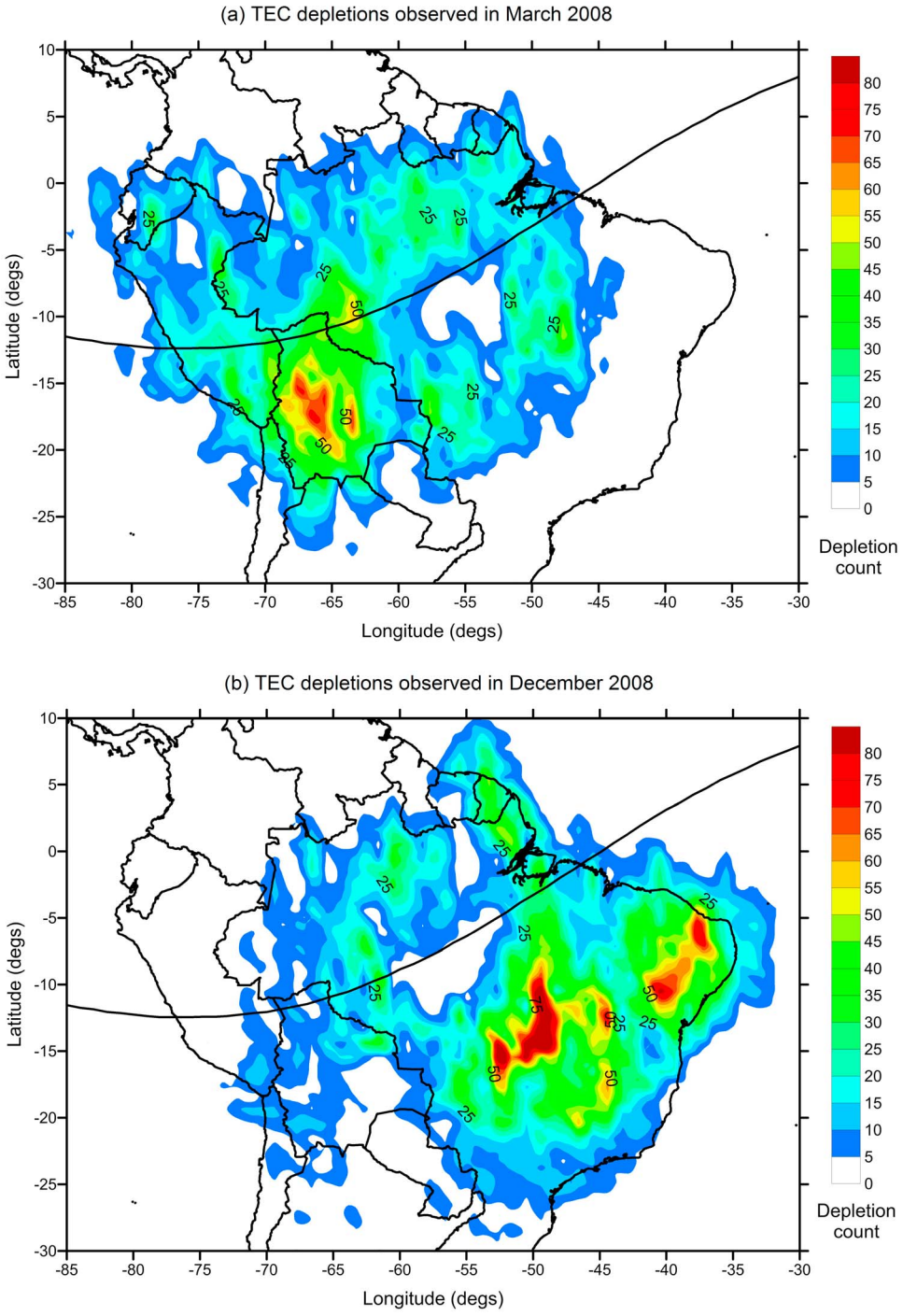

Figure 10. Total number of depletions detected spatially over South American continent for (a) the equinoxial month of March 2008 and (b) the solstice month of December 2008.

4.2. Statistical Analysis of TEC Depletion Depth, East-West Extension and Local Time

[31] The east-west extent and the depth of the TEC depletions observed by transiting GPS satellites are important parameters to measure as wider and/or deeper depletions produce system failure effects on GPS-based navigation systems that may operate in South America. During the low solar activity year of 2008, a total of 91,280 TEC depletions were detected by our analysis algorithm based on recordings from 127 GPS receivers that operated across the continent. Using this unique database, we have constructed histograms categorizing the depth of the TEC depletions in TEC units, the east-west extent of the depletions in minutes, and the local time the depletions. These histograms are presented in Figures 12a, 12b and 12c, respectively. It should be noted that each one of these depletions maybe is counted more than

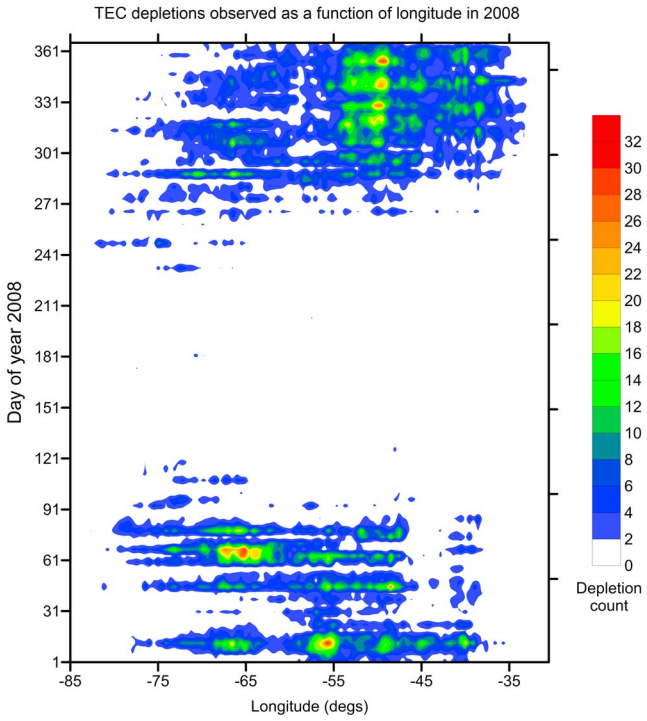

Figure 11. Observation of TEC depletions as a function of longitude, identified from all stations in South American region for the year of 2008.

once since different line of sights from different ground receivers and different GPS satellites can pierce the same depletion.

[32] The histogram of Figure 12a indicates that the most probable depth of the depletions varies from 2 to 5 TEC units which is nominal in South America during the minimum solar cycle. However, during the peak of solar cycle we expect that the depth of depletions will be much larger than what is shown in this figure. It is known that the ionosphere causes a group delay of 0.162 m per TEC unit at the GPS L1 frequency of 1.57542 GHz [*Warnant*, 1997; *Klobuchar et al.*, 1993], thus the presence of TEC depletions with an average depth of 5 TEC units will introduce range errors close to 1 m when the pass is near overhead. This error will increase at lower elevation angles.

[33] The histogram in Figure 12b shows the east-west time extent of the TEC depletions. It is important to mention that the parameter presented here does not represent the bubble duration or its lifetime but a measurement associated with their east-west size. As the GPS satellites move mainly in the north-south or south-north directions, taking 6 or more hours to move from horizon to horizon, it is possible to assume that the bubbles move across a quasi-stationary satellite-to-receiver line of sight. It can be seen from Figure 12b that the most probable east-west extensions of the depletions detected in South America are in the range of 15 to 35 min, with maximum number of depletions occurring around 25 min.

[34] Figure 12c displays the histogram for TEC depletions observed (in percentage of the total number of depletions) as a function of local time and sorted in bins of 30 min. The local times displayed here correspond to times when the plasma bubble was intercepted by the GPS signals. The occurrence number is highest between 2030 and 2330 LT, and there exists a gradual decrease of the depletion activity after local midnight, reaching low values at 0300 LT. We observe that the maximum onset probability is concentrated around 2130 LT in 2008. The shape of the local time distribution curve is similar to Figure 8 presented by *Burke et al.* [2004] based on satellite observations of equatorial plasma bubbles.

5. Discussion

[35] This paper presents the results of the first systematic study of TEC depletions observed across the South American continent. The depletion maps presented here have a continuity of over 45° in longitude (i.e., from 35°W to 80°W longitude) and over 40° in latitude on both sides of the magnetic equator. We also introduce for the first time the day-to-day variability of TEC depletions encompassing South America for a year of low solar activity. Section 3 presents individual plots of depletions to exemplify how the regional pattern of depletions varies seasonally and especially how their longitudinal extension contains a marked day-to-day variability. It is well known that the occurrence characteristics

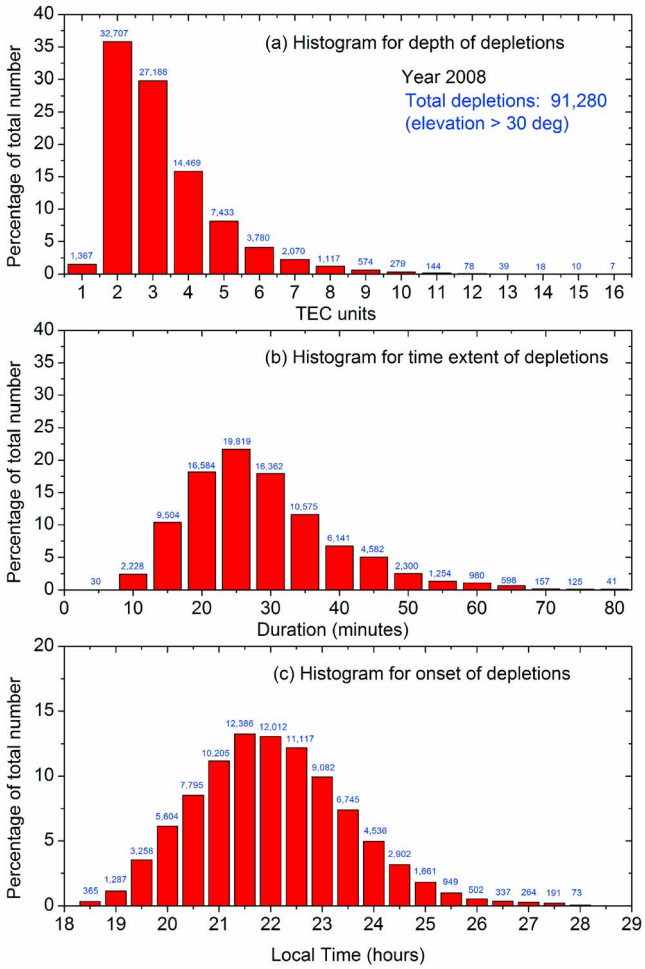

Figure 12. The depletion histograms of (a) depletion depth in TEC units, (b) time extent of depletions and (c) local time occurrence for the year of 2008 from all stations in the South American region.

of plasma depletions depend strongly on season and longitude [*Aarons*, 1993; *Huang et al.*, 2001; *Conker et al.*, 2004]. The statistics presented in this paper agrees with previous publications, but at the same time our analysis indicates that the longitudinal extension of regions populated with TEC depletions can change dramatically on a daily basis.

[36] It is evident that the characteristics of TEC depletion development follow closely the occurrence of ESF events, as both phenomena are related to the onset of plasma bubbles in the post-sunset equatorial F layer. The former is observed by in situ satellite measurements or ground-based receivers and the latter is observed as coherent echoes [*Woodman and LaHoz*, 1976] or on ionograms due to backscatter from the bottomside of the nighttime F layer. One of the most successful explanations for ESF activity to date is based on a hypothesis that ESF activity increases, when the solar terminator aligns with the geomagnetic field [*Tsunoda*, 1985]. We follow the terminology introduced by *Tsunoda* [2010a] and refer to it as the STBA hypothesis. The STBA hypothesis states that the occurrence frequency of equatorial ESF will be higher in the equinoxes than in the solstices except in regions where the magnetic declination is largely westward (December solstice) or eastward (June solstice).

[37] Comparison of Figures 10a and 10b reveals that the peak number of TEC depletions is 30% larger in the December solstice (78) than the number of depletions observed during the March equinox (60). We verified that during these two months, the number of satellite passes is about the same. The statistics of TEC depletions of Figures 10 and 11 follows closely the longitudinal occurrence pattern presented by *Burke et al.* [2004] for the South American longitudes. It also follows the STBA hypothesis as the maximum number of depletions is present in the western part of South America during the equinoctial months, and in the eastern longitudes (Brazilian sector) during the December solstice months. However, as indicated above, there are several days in the equinoxes as well as in solstice when the depletions are seen at all longitudes (see Figures 5a, 5b, 7a, and 7b).

[38] Figure 11 indicates that there are almost no depletions in the June solstice (except for a few events during June 2008). This is the period when the ITCZ moves farther away from the magnetic equator and no convective systems can trigger gravity waves (GWs) [*Tsunoda*, 2010a]. The June solstice is also the period when smaller PRE are registered in the America sector [*Fejer et al.*, 1999].

[39] It has been indicated that perturbations in the neutral gas such as GWs stimulate a response in plasma density only when there is alignment in the phase fronts of GWs with the magnetic field $\boldsymbol{B}$ lines [*Huang and Kelley*, 1996]. This conjecture has been referred by *Tsunoda* [2010a] as the gravity wave B alignment (GWBA) hypothesis. In the South American region, GWs can be triggered by mesoscale convective systems, which are usually found within the intertropical convergence zone (ITCZ). Based on this argument, several authors have concluded that the ESF morphology could be controlled by the seasonal migration of the ITCZ in latitude [*Röttger* 1977, 1981; *McClure et al.* 1998, *Tsunoda*, 2010b]. GWBA operates when the ITCZ is closer to the magnetic equator during the December solstice in South America. According to *Tsunoda* [2010b] the occurrence of ESF is attributable to two effects, STBA and GWBA, which appear to operate effectively during equinox and solstice respectively in the western side of South America. These hypotheses hold well for the climatology of TEC depletions on a monthly and seasonal basis. But, they do not explain the day to day variability of depletions that in certain occasions are observed at all longitudes in the South American continent either in equinoxes or solstice. To explain these features, we will need to consider the day-to-day variability of the ITCZ or the action of other mechanisms that can seed plasma bubbles all over the continent.

[40] Recently, *Woodman* [2009] has indicated that gravity wave seeding is not the only mechanism able to seed plasma bubbles; eastward neutral winds in regions of westward plasma flows, as happens at the bottom of the *F* region right after sunset, can generate the proper conditions for bubbles to develop [*Kudeki et al.*, 2007]. The eastward zonal winds are responsible for the pre-reversal enhancement (PRE) of the vertical velocities and the consequent uplift of the F-layer to the more unstable higher altitudes. They can also drive 10s of km scale density waves with wavefronts tilted 45° to the west during the initial phase of the post-sunset vortex [*Kudeki et al.*, 2007]. These waves can serve as seeds for the larger scale plasma bubbles. *Hysell and Kudeki* [2004] has also discussed the role of the collisional shear instability in seeding equatorial spread F based upon the fact that strong shears exists in the bottomside equatorial F region ionosphere around twilight, where the plasma flow in the bottomside reverses from westward to eastward with increasing altitude [*Kudeki et al.*, 1981; *Tsunoda et al.*, 1981]. Shear flow develops in the equatorial ionosphere beginning around 14 LT each day and intensifies at twilight as the E and valley regions recombine. Despite having a modest growth rate, shear instabilities may therefore undergo several e-folds before interchange instabilities activate and thereby create the seed irregularities necessary for full blown spread F to occur. To resolve which one of these mechanisms is responsible for the day-to-day variability of TEC depletions will require the use of daily maps of meso-scale convection systems over the South American continent or a database of zonal winds measured by the existent Fabry-Perot instruments that are presently operating in the continent.

[41] To the extent any ionospheric instability amplifies geophysical noise, and the gravity waves probably do constitute a significant part of atmospheric geophysical noise, many aspects of the conjecture seem plausible. Which of these factors are most important remains to be known, either neutral wind or factors that are thought to contribute to shear flow, including E region dynamo winds, vertical winds and horizontal electric fields on flux tubes with significant Hall conductivity, and vertical currents sourced in the electrojet region near the solar terminator [*Haerendel et al.*, 1992; *Haerendel and Eccles*, 1992], in part because they are difficult to measure directly using in situ or remote sensing. These different mechanisms, as the ones described above, do not necessarily require gravity waves as the seeding mechanism; they may be acting following an unknown pattern, increasing the day-to-day variability of the ESF phenomena.

[42] The statistics of TEC depletion depths (Figure 12a) for 2008 show that the highest probable depths are low in the range of 2 to 3 TEC units; this could be attributed to the low solar activity year with average F10.7 solar radio flux of 69.0. Year 2008 was the quietest year of the space age with

266 days of no visible sunspots, according to National Oceanic and Atmospheric Administration (NOAA). *Rama Rao et al.* [2006] found the most probable TEC depths of about 5 to 15 TEC units during the month of March 2004 (monthly average F10.7 flux is 112.16) over the India region, during the descending phase of the solar cycle. The difference in TEC depletion depths between the Indian region and South America is more attributable to the solar activity than the geographic difference per se. From the histogram of depletion extent in minutes it can be seen that the most probable depletion duration intercepted by the GPS satellites are in the range of 15 to 35 min, while the local time onset of depletions are found to be in range of 1930 to post midnight 0030 LT.

6. Summary

[43] This paper presents the day-to-day variability of the TEC depletions over the South American continent for the entire year of 2008. Observations of depletions in this year of low solar activity show that the seasonal and longitudinal variability is comparable to that obtained by *Burke et al.* [2004] based on in situ satellite measurements.

[44] It can be concluded that the climatology of depletions agree with *Tsunoda*'s [2010b] hypothesis on the STBA and GWBA. However, the day-to-day variability cannot be easily reconciled with these theories. The statistics of TEC depletions depths show that in 2008, the most probable depths are small in the range of 2 to 3 TEC units and the most likely time extents are in the range of 15 to 35 min, with maximum local time occurrence falling around 2130 local time hours.

[45] The day-to-day variability that stands out of the usual seasonal and longitudinal pattern for the occurrence of equatorial plasma depletions may be explained by the following two possible mechanisms:

[46] According to *Kudeki and Bhattacharyya* [1999] and *Kudeki et al.* [2007] the eastward neutral winds play a primary role rather than gravity waves in triggering the equatorial spread F that could lead to formation of plasma depletions.

[47] *Tsunoda* [2010a, 2010b] postulated that the gravity waves generated by mesoscale convective systems, which are usually found within the ITCZ are responsible for the seeding mechanisms for plasma depletions. We may assume that the day-to-day variability in the occurrence of TEC depletions may be related to the day to day variability in location of ITCZ with respect to the magnetic equator. This investigation of the possible relationship between the day-to-day variability in plasma depletions and ITCZ requires further study.

[48] **Acknowledgments.** The authors would like to thank International GNSS service (IGS), Geocentric Reference System for the Americas (SIRGAS) and Michael Bevis from Ohio State University - Central and Southern Andes GPS Project (OSU-CAP) for providing GPS data. C.E.V. was partially supported by Air Force Research Laboratory contract FA8718-09-C-0041 and NSF grant ATM-0521487. Low Latitude Ionospheric Sensor Network (LISN) is a project led by Boston College in collaboration with the Geophysical Institute of Peru, and other institutions that provide information in benefit of the scientific community. We thank all organizations and persons that are supporting and operating receivers in LISN. We thank our colleagues Patricia Doherty, Endowake Yizengaw and Robert Sheehan for their helpful comments and suggestions on the paper.

References

Aarons, J. (1993), The longitudinal morphology of equatorial *F* layer irregularities relevant to their occurrence, *Space Sci. Rev.*, *63*, 209–243, doi:10.1007/BF00750769.

Basu, S., et al. (1996), Scintillations, plasma drifts, and neutral winds in the equatorial ionosphere after sunset, *J. Geophys. Res.*, *101*(A12), 26,795–26,809, doi:10.1029/96JA00760.

Basu, Su., et al. (2005), Two components of ionospheric plasma structuring at midlatitudes observed during the large magnetic storm of October 30, 2003, *Geophys. Res. Lett.*, *32*, L12S06, doi:10.1029/2004GL021669.

Brunini, C., L. Sánchez, H. Drewes, S. Costa, V. Mackern, W. Martínez, W. Seemüller, and A. da Silva (2011), Improved analysis strategy and accessibility of the SIRGAS Reference Frame, in *Geodesy for Planet Earth Proceedings of the 2009 IAG Symposium, Buenos Aires, Argentina, 31 August 31–4 September 2009*, *Int. Assoc. Geod. Symp.*, vol. 136, edited by S. Kenyon, M. C. Pacino, and U. Marti, Springer, New York, in press.

Burke, W. J., L. C. Gentile, C. Y. Huang, C. E. Valladares, and S. Y. Su (2004), Longitudinal variability of equatorial plasma bubbles observed by DMSP and ROCSAT-1, *J. Geophys. Res.*, *109*, A12301, doi:10.1029/2004JA010583.

Conker, R. S., M. B. El-Arini, R. Lejeune, P. Doherty, and C. Valladares (2004), Description of a real-time algorithm for detecting ionospheric depletions for SBAS and the statistics of depletions in South America during the peak of the current solar cycle, paper presented at Beacon Satellite Symposium (BSS), Beacon Satell. Stud. Group, Trieste, Italy.

DasGupta, A., S. Basu, J. Aarons, J. A. Klobuchar, Su. Basu, and A. Bushby (1983), VHF amplitude scintillations and associated electron content depletions as observed at Arequipa, Peru, *J. Atmos. Terr. Phys.*, *45*, 15–26, doi:10.1016/S0021-9169(83)80003-8.

Dow, J. M., R. E. Neilan, and C. Rizos (2009), The International GNSS Service in a changing landscape of Global Navigation Satellite Systems, *J. Geod.*, *83*, 191–198, doi:10.1007/s00190-008-0300-3.

Fejer, B., L. Scherliess, and E. de Paula (1999), Effects of the vertical plasma drift velocity on the generation and evolution of equatorial spread *F*, *J. Geophys. Res.*, *104*, 19,859–19,869, doi:10.1029/1999JA900271.

Foster, J. C., et al. (2005), Multiradar observations of the polar tongue of ionization, *J. Geophys. Res.*, *110*, A09S31, doi:10.1029/2004JA010928.

Haerendel, G., and J. V. Eccles (1992), The role of the equatorial electrojet in the evening ionosphere, *J. Geophys. Res.*, *97*, 1181–1192, doi:10.1029/91JA02227.

Haerendel, G., J. V. Eccles, and S. Cakir (1992), Theory for modeling the equatorial evening ionosphere and the origin of the shear in the horizontal plasma flow, *J. Geophys. Res.*, *97*, 1209–1223, doi:10.1029/91JA02226.

Ho, C. M., A. J. Mannucci, L. Sparks, X. Pi, U. L. Lindqwister, B. D. Wilson, B. A. Iijima, and M. J. Reyes (1998), Ionospheric total electron content perturbations monitored by the GPS global network during two Northern Hemisphere winter storms, *J. Geophys. Res.*, *103*, 26,409–26,420, doi:10.1029/98JA01237.

Huang, C. S., and M. C. Kelley (1996), Nonlinear evolution of equatorial spread *F*: 2. Gravity wave seeding of Rayleigh-Taylor instability, *J. Geophys. Res.*, *101*, 293–302, doi:10.1029/95JA02210.

Huang, C. Y., W. J. Burke, J. S. Machuzak, L. C. Gentile, and P. Sultan (2001), DMSP observations of equatorial plasma bubbles in the topside ionosphere near solar maximum, *J. Geophys. Res.*, *106*, 8131–8142, doi:10.1029/2000JA000319.

Hysell, D. L., and J. Burcham (1998), JULIA radar studies of equatorial spread *F*, *J. Geophys. Res.*, *103*, 29,155–29,167, doi:10.1029/98JA02655.

Hysell, D. L., and E. Kudeki (2004), Collisional shear instability in the equatorial *F* region ionosphere, *J. Geophys. Res.*, *109*, A11301, doi:10.1029/2004JA010636.

Klobuchar, J. A., S. Basu, and P. Doherty (1993), Potential limitations in making absolute ionospheric measurements using dual frequency radio waves from GPS satellites, paper presented at Ionospheric Effects Symposium, Air Force Res. Lab., Boston, Mass., May.

Kudeki, E., and S. Bhattacharyya (1999), Postsunset vortex in equatorial *F*-region plasma drifts and implications for bottomside spread-*F*, *J. Geophys. Res.*, *104*, 28,163–28,170, doi:10.1029/1998JA900111.

Kudeki, E., B. G. Fejer, D. T. Farley, and H. M. Ierkic (1981), Interferometer studies of equatorial *F* region irregularities and drifts, *Geophys. Res. Lett.*, *8*, 377, doi:10.1029/GL008i004p00377.

Kudeki, E., A. Akgiray, M. Milla, J. L. Chau, and D. L. Hysell (2007), Equatorial spread-*F* initiation: Post-sunset vortex, thermospheric winds, gravity waves, *J. Atmos. Sol. Terr. Phys.*, *69*, 2416–2427, doi:10.1016/j.jastp.2007.04.012.

Lee, J. K., F. Kamalabadi, and J. J. Makela (2007), Localized three-dimensional ionospheric tomography with GPS ground receiver measurements, *Radio Sci.*, *42*, RS4018, doi:10.1029/2006RS003543.

Lee, J. K., F. Kamalabadi, and J. J. Makela (2008), Three-dimensional tomography of ionospheric variability using a dense GPS receiver array, *Radio Sci.*, *43*, RS3001, doi:10.1029/2007RS003716.

Ma, X. F., T. Maruyama, G. Ma, and T. Takeda (2005), Three-dimensional ionospheric tomography using observation data of GPS ground receivers and ionosonde by neural network, *J. Geophys. Res.*, *110*, A05308, doi:10.1029/2004JA010797.

McClure, J., S. Singh, D. Bamgboye, F. Johnson, and H. Kil (1998), Occurrence of equatorial *F* region irregularities: Evidence for tropospheric seeding, *J. Geophys. Res.*, *103*, 29,119–29,135, doi:10.1029/98JA02749.

Mitchell, C. N., and P. S. J. Spencer (2003), A three-dimensional time-dependent algorithm for ionospheric imaging using GPS, *Ann. Geophys.*, *46*(4), 687–696.

Portillo, A., M. Herraiz, S. M. Radicella, and L. Ciraolo (2008), Equatorial plasma bubbles studied using African slant total electron content observations, *J. Atmos. Sol. Terr. Phys.*, *70*, 907–917, doi:10.1016/j.jastp.2007.05.019.

Rama Rao, P. V. S., S. Gopi Krishna, K. Niranjan, and D. S. V. V. D. Prasad (2006), Study of spatial and temporal characteristics of L-band scintillations over the Indian low-latitude region and their possible effects on GPS navigation, *Ann. Geophys.*, *24*, 1567–1580, doi:10.5194/angeo-24-1567-2006.

Röttger, J. (1977), Travelling disturbances in the equatorial ionosphere and their association with penetrative cumulus convection, *J. Atmos. Terr. Phys.*, *39*, 987, doi:10.1016/0021-9169(77)90007-1.

Röttger, J. (1981), Equatorial spread *F* by electric fields and atmospheric gravity waves generated by thunderstorms, *J. Atmos. Terr. Phys.*, *43*, 453, doi:10.1016/0021-9169(81)90108-2.

Saito, A., S. Fukao, and S. Miyazaki (1998), High resolution mapping of TEC perturbations with the GSI GPS network over Japan, *Geophys. Res. Lett.*, *25*, 3079–3082, doi:10.1029/98GL52361.

Sardón, E., and N. Zarraoa (1997), Estimation of total electron content using GPS data: How stable are the differential satellite and receiver instrumental biases?, *Radio Sci.*, *32*(5), 1899–1910, doi:10.1029/97RS01457.

Shiokawa, K., Y. Otsuka, T. Ogawa, N. Balan, K. Igarashi, A. J. Ridley, D. J. Knipp, A. Saito, and K. Yumoto (2002), A large-scale traveling ionospheric disturbance during the magnetic storm of 15 September 1999, *J. Geophys. Res.*, *107*(A6), 1088, doi:10.1029/2001JA000245.

Tsunoda, R. (1985), Control of the seasonal and longitudinal occurrence of equatorial scintillations by the longitudinal gradient in integrated *E* region Pedersen conductivity, *J. Geophys. Res.*, *90*, 447–456, doi:10.1029/JA090iA01p00447.

Tsunoda, R. T. (2010a), On seeding equatorial spread *F* during solstices, *Geophys. Res. Lett.*, *37*, L05102, doi:10.1029/2010GL042576.

Tsunoda, R. T. (2010b), On equatorial spread *F*: Establishing a seeding hypothesis, *J. Geophys. Res.*, *115*, A12303, doi:10.1029/2010JA015564.

Tsunoda, R. T., R. C. Livingston, and C. L. Rino (1981), Evidence of a velocity shear in bulk plasma motion associated with the post-sunset rise of the equatorial *F* layer, *Geophys. Res. Lett.*, *8*, 807–810, doi:10.1029/GL008i007p00807.

Valladares, C. E., S. Basu, K. Groves, M. Hagan, D. Hysell, A. Mazzella Jr., and R. Sheehan (2001), Measurement of the latitudinal distributions of total electron content during equatorial spread F events, *J. Geophys. Res.*, *106*, 29,133–29,152, doi:10.1029/2000JA000426.

Valladares, C. E., J. Villalobos, R. Sheehan, and M. P. Hagan (2004), Latitudinal extension of low-latitude scintillations measured with a network of GPS receivers, *Ann. Geophys.*, *22*, 3155–3175, doi:10.5194/angeo-22-3155-2004.

Valladares, C. E., J. Villalobos, M. A. Hei, R. Sheehan, Su. Basu, E. MacKenzie, P. H. Doherty, and V. H. Rios (2009), Simultaneous observation of travelling ionospheric disturbances in the Northern and Southern Hemispheres, *Ann. Geophys.*, *27*, 1501–1508, doi:10.5194/angeo-27-1501-2009.

Warnant, R. (1997), Reliability of the TEC computed using the GPS measurements: The problem of hardware biases, *Acta Geod. Geophys. Hung.*, *32*(3–4), 451–459.

Weber, E., et al. (1996), Equatorial plasma depletion precursor signatures and onset observed at 11° south of the magnetic equator, *J. Geophys. Res.*, *101*, 26,829–26,838, doi:10.1029/96JA00440.

Woodman, R. F. (2009), Spread F–an old equatorial aeronomy problem finally resolved?, *Ann. Geophys.*, *27*, 1915–1934, doi:10.5194/angeo-27-1915-2009.

Woodman, R. F., and C. LaHoz (1976), Radar observations of *F* region equatorial irregularities, *J. Geophys. Res.*, *81*, 5447, doi:10.1029/JA081i031p05447.

Yeh, K. C., H. Soicher, C. H. Liu, and E. Bonelli (1979), Ionospheric bubbles observed by the Faraday rotation method at Natal, Brazil, *Geophys. Res. Lett.*, *6*, 473–475, doi:10.1029/GL006i006p00473.

G. K. Seemala and C. E. Valladares, Institute for Scientific Research, St. Clements Hall 414, Boston College, Chestnut Hill, MA 02467, USA. (gopi.seemala@bc.edu; cesar.valladares@bc.edu)